UROGENITAL IMAGING
Iran J Radiol. 2021 October; 18(4):e110963. doi: 10.5812/iranjradiol.110963.
Published online 2021 October 11. **Research Article**

Use of Histogram Analysis in Diffusion-Weighted Magnetic Resonance Imaging for Differentiation of Renal Tumor Subgroups

Gurcan Erbay [1], Mehmet Resit Goren [2,*], Elif Karadeli [1], Burcak Pekoz [3], Zafer Koc [1] and Sami Arica [4]

[1]Department of Radiology, Baskent University School of Medicine, Adana Dr. Turgut Noyan Medical and Research Center, Adana, Turkey
[2]Department of Urology, Baskent University School of Medicine, Adana Dr. Turgut Noyan Medical and Research Center, Adana, Turkey
[3]Department of Radiology, Adana City Hospital, Adana, Turkey
[4]Department of Electrical and Electronics Engineering, Cukurova University Faculty of Engineering and Architecture, Adana, Turkey

[*]*Corresponding author*: Department of Urology, Baskent University School of Medicine, Adana Dr. Turgut Noyan Medical and Research Center, Adana, Turkey. Email: mrgoren@baskent.edu.tr

Received 2020 December 12; **Revised** 2021 July 03; **Accepted** 2021 August 28.

Abstract

Background: The histopathological differentiation of renal neoplasms can be challenging via imaging.
Objectives: To evaluate differences in histogram parameters on apparent diffusion coefficient (ADC) maps and to investigate the efficacy of histogram analysis in differentiation of oncocytomas from malignant renal neoplasm (MRN) subgroups.
Patients and Methods: In this cross-sectional, retrospective study, the texture parameters of diffusion-weighted magnetic resonance images (DW-MRI) were evaluated in 65 patients with renal tumors (nine cases of oncocytoma and 59 cases of MRN) for a histological analysis.
Results: A total of 68 lesions from 50 male and 15 female patients, with a median age of 55.4 years, were examined in this study. There were significant differences in the mean, median, and peak ADC values, as well as ADC percentiles, between the oncocytoma and MRN subgroups. Regarding the histopathological features of the lesions, 9 (11.5%) cases of oncocytomas, 23 (29.5%) cases of clear cell renal carcinoma (ccRCC), 14 (17.9%) cases of papillary renal cell carcinoma (pRCC), 12 (15.4%) cases of chromophobe renal cell carcinoma (chRCC), and 10 (12.8%) other tumors (including four cases of transitional cell carcinoma, four cases of non-Hodgkin's lymphoma, and two cases of primitive neuroectodermal tumor) were identified. Significant differences were found in the mean and median ADC values between the oncocytoma, pRCC, chRCC, and other MRN subgroups. Moreover, significant differences were found in the mean and median ADC values between the ccRCC, pRCC, and chRCC subgroups. There were also significant differences in the percentiles of mean and median ADCs between oncocytomas and pRCC, chRCC, and other MRN subgroups. However, there were no significant differences in the mean and median ADCs (including the percentile histogram analysis) or the peak ADC between the oncocytoma and ccRCC groups. The mean, median, and percentile of ADC for renal masses were superior to kurtosis, skewness, and entropy.
Conclusion: Although differentiation between ccRCC and oncocytoma was not possible by only measuring the mean, median, and peak ADC values, the histogram analysis of ADCs may improve differentiation between the MRN subgroups. Clearly, ADC cannot be used to differentiate between oncocytomas and MRNs.

Keywords: Magnetic Resonance Imaging, Diffusion, Renal Cell Carcinoma, Histogram Analysis

1. Background

The incidence of renal neoplasms is 2 - 3% of all cancers. The most common renal tumors include oncocytomas, angiomyolipoma (AML), clear cell carcinoma, papillary carcinoma, chromophobe renal cell carcinoma (chRCC), non-Hodgkin's lymphoma (NHL), and transitional cell cancer (TCC) (1). The histopathological differentiation of renal neoplasms can be challenging by using imaging modalities. Ultrasonography (USG) and computed tomography (CT) scan are commonly used diagnostic modalities to detect AML lesions with a high fat content. Besides, magnetic resonance imaging (MRI) is particularly useful for distinguishing AML lesions with low lipid content (2, 3).

On the other hand, renal oncocytomas do not have characteristic features on CT, USG, intravenous urography, or MRI. Also, the efficacy of fine-needle aspiration in the diagnosis of oncocytomas is controversial and restricted, because there may be no characteristic features to distinguish oncocytomas from renal cell carcinomas (RCCs)

(4). Therefore, it is important to distinguish renal oncocytomas from RCCs to prevent unnecessary surgical interventions. Commonly, a visual or qualitative evaluation of tumor contrast enhancement is performed using CT and MRI for differentiation of tumor subtypes. It is known that contrast enhancement of clear cell renal carcinoma (ccRCC) is more extensive than papillary renal cell carcinomas.

Nevertheless, contrast enhancement and region of interest (ROI) methods have restrictions, including interobserver variability in ROI placement, misregistration between pre- and post-contrast images, and ROI placement difficulties in pre-contrast images for T1-isointense intrarenal tumors. However, the combined use of these two methods has shown high accuracy in differentiating ccRCC from papillary renal cell carcinoma (pRCC). There are several restrictions, including interobserver variability in ROI placement, misregistration between pre- and post-contrast acquisitions, and difficult ROI placement in an unenhanced image for a T1-isointence intrarenal tumor (5).

Image heterogeneity is a common problem, and judgement by a single radiologist is likely to be subjective. However, these shortcomings can be overcome by using texture features in a quantitative computer-aided analysis. Kurtosis and skewness, as first-order histogram distribution parameters, represent tumor heterogeneity. Second-order texture parameters, including co-occurrence matrix measures, represent the distribution of co-occurring gray-scale values. Recently, texture analysis has been used for some organs, including the breasts, brain, and prostate, to differentiate benign lesions from malignant lesions (6-9).

The apparent diffusion coefficient (ADC) provides information on the free motion of water molecules. It involves different features, such as microcirculation, blood viscosity, cellularity, and cell membrane integrity. A decreased ADC value refers to restricted diffusion, which is observed in malignant tumors (10-12). Both diffusion-weighted imaging (DWI) with quantitative ADC measurement and contrast-enhanced MRI have shown high efficacy in differentiating RCC subtypes and other tumors involving the kidneys, such as oncocytomas, TCC, and NHL.

2. Objectives

This study aimed to examine differences in histogram parameters on ADC maps and to investigate their applicability in differentiating oncocytomas from malignant renal neoplasms (MRNs).

3. Patients and Methods

This cross-sectional study was approved by our institutional review board (Project No.: KA15/199). The records of urology, radiology, and pathology departments were retrospectively reviewed between January 2014 and December 2019. A total of 75 patients with preoperative abdominal DW-MRI were included in this study. None of the patients received any treatments before surgery.

The pathological diagnosis of the lesions was as follows: 9 (11.5%) cases of oncocytomas, 23 (29.5%) cases of ccRCC, 14 (17.9%) cases of pRCC, 12 (15.4%) cases of chRCC, and 10 (12.8%) other tumors (four cases of TCC, four cases of NHL, and two cases of primitive neuroectodermal tumor [PNET]). Eight lesions, which were identified as cystic RCC tumors with extensive cystic necrotic areas (> 50% of tumors), and two lesions, which were identified as lipid-poor AMLs, were excluded from the analysis. Finally, 68 lesions were evaluated in this study.

3.1. MRI Technique

All patients were evaluated via renal MRI, using a 1.5 T torso phased array coil (Avanto, Siemens, Germany). The MRI protocol included coronal and transverse half-Fourier acquisition single-shot turbo spin echo (HASTE) images, transverse in- and opposed-phase gradient-echo T1-weighted images, and dynamic 3D fat-suppressed gradient-echo T1-weighted images before and after the intravenous administration of gadoteric acid at a single dose of 0.1 mmol/kg (Dotarem, Guerbet, France). Transverse DW-MRI was performed with b-values of 0, 200, 600, and 1000 s/mm^2, and fat-suppressed single-shot echo-planar imaging was performed with three-directional motion-probing gradients.

The DWI sequence parameters were as follows: repetition time (TR), 4600 - 4800 ms; echo time (TE), 80 - 90 ms; number of excitations (NEX), 4; parallel imaging factor, 2; section thickness, 4 mm; matrix size, 192 $\times$ 128; and field of view (FOV), 377 mm. The acquisition time changed depending on the patient's respiratory cycle in respiratory-triggered DWI. The mean acquisition time was 140 seconds. The ADC maps were plotted automatically on a Leonardo workstation (Siemens Healthineers, Germany), together with the b-values.

3.2. Image Texture Analysis

MATLAB® technical computing software (MathWorks, Inc., Natick, Massachusetts, USA) was used for the quantitative analysis of ADC maps. The tumor types were not known prior to the analyses. In the evaluation phase of lesions on the ADC maps, ROI was drawn right inside the outer margin of the lesion to avoid partial volume errors, and then, the volume of interest (VOI) was measured for the lesion. The superior and inferior slices of the lesion were removed to eliminate the effect of average volume.

For the VOI of each lesion, an in-house software was used to quantify the mean ADC values. Skewness and kurtosis were also computed from the histogram, with a bin width of $\times 10^{-5}$ mm^2/s for the VOI of each lesion. The VOI placement for the lesions and the texture parameters were also evaluated using MATLAB® 7.13 (R2011b, MathWorks, Inc., Natick, Massachusetts, USA); the examination took 5 - 7 minutes per lesion. An example of VOI placement is presented in Figure 1.

The ADC histograms were plotted on the x-axis with a bin size of 1×10^6 mm/sec, and the percentage of the total lesion volume was calculated by dividing the frequency in each bin by the total number of voxels on the y-axis. A cumulative analysis was also performed with the ADC histograms, where the cumulative number of observations in all bins, up to the specified bin, was mapped onto the y-axis (expressed as percentage) (6).

3.3. Statistical Analysis

Statistical analysis was performed in SPSS version 17.0 (SPSS Inc., Chicago, IL, USA). If continuous variables had a normal distribution, they were described as mean ± standard deviation ($P > 0.05$ in Kolmogorov-Smirnov test or Shapiro-Wilk; $n < 30$); otherwise, if continuous variables were not normally distributed, they were described as median values. Comparisons between the groups were performed using Student's *t*-test or one-way analysis of variance (ANOVA) for normally distributed variables, while Mann-Whitney U test or Kruskal-Wallis test was used for variables without a normal distribution. A receiver operating characteristic (ROC) curve analysis was performed, and the area under the curve (AUC), as well as sensitivity (sens) and specificity (spec) were calculated. P-values less than 0.05 were considered statistically significant.

4. Results

This study was conducted on 50 male and 15 female patients. The median age of the cohort was 55.4 years (range: 41 - 69 years). The mean size of oncocytomas and MRNs was 5.15 ± 3.33 and 5.04 ± 3.85 cm, respectively. Table 1 summarizes the quantitative first-order texture features on the ADC maps. The mean ADCs of oncocytomas were significantly different from those of MRNs ($1.808 \times 10^{-3} \pm 0.44 \times 10^{-3}$ mm^2/s vs. $1.319 \times 10^{-3} \pm 0.35 \times 10^{-3}$ mm^2/s; P = 0.001). Besides, there were significant differences in the median and peak ADC values of the ADC histogram between the oncocytomas and MRNs (Table 1).

The cutoff values for the mean and median ADCs for differentiation of oncocytomas from MRNs were 1.466×10^{-3} and 1.431×10^{-3} mm^2/s, respectively. The cutoff value for the mean ADC showed a sensitivity of 75% and a specificity of 70%. Also, the cutoff value for the median ADC showed a sensitivity of 73% and a specificity of 67%. The AUC for the mean and median ADCs was 0.826 and 0.821, respectively. The 5th, 10th, 20th, 30th, 40th, 50th, 60th, 70th, 80th, 90th, and 95th percentiles of the mean and median ADCs also showed significant differences between the oncocytomas and MRNs ($P < 0.05$).

Table 2 presents a comparison of kurtosis, skewness, and entropy with the mean and median ADC values for different tumor types on ADC images. The kurtosis was lower in oncocytomas compared to MRNs on ADC images (7.77 ± 1.59 vs. 9.22 ± 3.9), although the difference was not significant (P = 0.47). There was no significant difference in skewness between oncocytomas and MRNs (2.22 ± 0.30 vs. 2.41 ± 0.67; P = 0.47). Entropy was also similar between the oncocytomas and MRN subgroups (4.95 ± 0.31 vs. 4.79 ± 0.54; P = 0.42).

There were no significant differences in the mean and median ADC values of oncocytomas and ccRCC (P = 0.176 and P = 0.190, respectively) (Table 3). However, the mean and median ADC values of oncocytomas differed significantly from those of pRCC, chRCC, and other tumors. Besides, significant differences were found in the mean and median ADC values of ccRCC with pRCC, chRCC, and other tumor subgroups ($P < 0.05$). Nevertheless, there was no significant difference in the peak ADC values between the oncocytomas and ccRCC ($P > 0.05$). Conversely, significant differences were found in the peak ADC values between the oncocytomas and pRCC, chRCC, and other tumors ($P < 0.05$). Also, the peak ADC was significantly different between the ccRCC, pRCC, chRCC, and other tumors ($P < 0.05$).

Comparison of the 5th, 10th, 20th, 30th, 40th, 50th, 60th, 70th, 80th, 90th, and 95th percentiles of the mean and median ADC values showed significant differences between the oncocytomas and pRCC, chRCC, and other tumors ($P < 0.05$). However, there was no significant difference between ccRCC and oncocytomas. Based on the results, there were significant differences between the ccRCC, pRCC, chRCC, and other tumor subtypes when the 5th, 10th, 20th, 30th, 40th, 50th, 60th, 70th, and 80th percentiles of the mean ADCs were compared ($P < 0.05$). However, there were no significant differences in the 90th and 95th percentiles of the mean ADC values between the ccRCC and other tumor types.

Moreover, the present results showed significant differences in the 5th, 10th, 20th, 30th, 40th, 50th, 60th, 70th, 80th, 90th, and 95th percentiles of the median ADC values between the ccRCC, pRCC, and chRCC subgroups ($P < 0.05$). Nevertheless, there was no significant difference in the kurtosis, skewness, or entropy on the ADC images be-

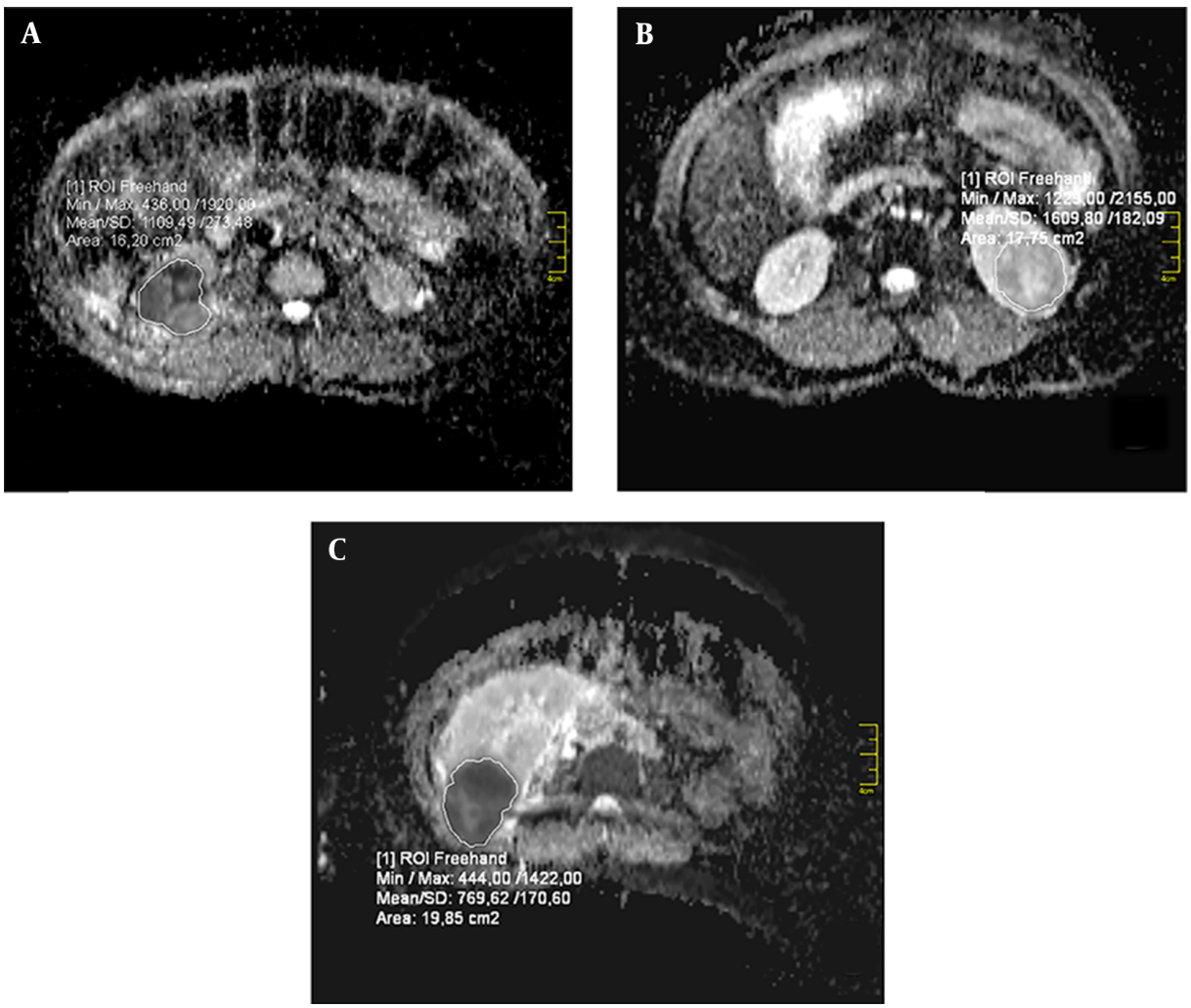

Figure 1. Magnetic resonance images of different renal tumors and placement of the region of interest (ROI). A, Clear cell renal cancer (ccRCC); B, Oncocytoma; and C, Primitive neuroectodermal tumor.

Table 1. Comparison of Apparent Diffusion Coefficient Histogram Analyses Between Oncocytomas and Malignant Renal Neoplasms [a]

ADC Maps	Kurtosis	Skewness	Entropy	Mean ADC	Median ADC
Oncocytoma	7.77 ± 1.59	2.22 ± 0.30	4.95 ± 0.31	1.808 ± 0.44	1.811.9 ± 0.44
MRN	9.22 ± 3.9	2.41 ± 0.67	4.79 ± 0.54	1.319 ± 0.35	1.315 ± 0.36
P-value	0.47	0.47	0.42	< 0.001	< 0.001

Abbreviations: ADC, apparent diffusion coefficient; MRNs, malignant renal neoplasms.
[a] Data are presented as mean ± SD.

Table 2. Comparison of Apparent Diffusion Coefficient Values and Histogram Analyses Between Renal Neoplasms [a]

Tumor types	Kurtosis	Skewness	Entropy	Mean ADC	Median ADC
Oncocytoma	7.71 ± 1.68	2.20 ± 0.30	4.99 ± 0.30	1839.1 ± 462.1	1842.2 ± 462.8
ccRCC	9.00 ± 3.75	2.41 ± 0.58	4.77 ± 0.49	1544.4 ± 391	1549.1 ± 399.9
pRCC	10.06 ± 3.75	2.55 ± 0.63	4.68 ± 0.54	1161.4 ± 260.8	1153.6 ± 255.8
chRCC	8.67 ± 2.70	2.40 ± 0.45	4.83 ± 0.39	1160.0 ± 231.2	1148.1 ± 232.2
Other MRNs	9.14 ± 6.03	2.25 ± 1.06	4.94 ± 0.80	1237.0 ± 224.1	1228.5 ± 238.0

Abbreviations: ADC, apparent diffusion coefficient; ccRCC, clear cell renal cell cancer; pRCC, papillary renal cell cancer; chRCC, chromophobe renal cell cancer; MRNs, malignant renal neoplasms.
[a] Data are presented as mean ± SD.

Table 3. P-Values for the Comparison of Mean and Median Apparent Diffusion Coefficient Values Between Oncocytomas and Clear Cell Renal Cell Cancer (ccRCC)

	ccRCC	pRCC	chRCC	Oncocytoma	Other MRNs
Oncocytoma, mean ADC	0.176	< 0.001	< 0.001	N/A	0.002
Oncocytoma, median ADC	0.19	< 0.001	< 0.001	N/A	0.002
ccRCC, mean ADC	N/A	0.010	0.016	0.176	0.119
ccRCC, median ADC	N/A	0.008	0.016	0.190	0.102

Abbreviations: ADC, apparent diffusion coefficient; ccRCC, clear cell renal cell cancer; pRCC, papillary renal cell cancer; chRCC, chromophobe renal cell cancer; MRNs, malignant renal neoplasms.

tween the tumor subgroups (oncocytoma, ccRCC, pRCC, chRCC, and other tumors).

5. Discussion

There are many challenges in the assessment and differentiation of renal neoplasms (except angiomyolipomas) using imaging modalities. In recent years, texture analysis in CT scan and MRI has been utilized for the assessment of different tumor types, including the brain, neck, breast, renal, cervix, prostate, and rectal tumors, as well as the assessment of treatment response. Besides, this type of analysis has been used to differentiate ccRCC from pRCC and to assess the RCC stage (7-12).

DWI has been used to distinguish benign renal lesions from malignant ones. The heterogeneity of vascular and tissue diffusion components may cause ADC heterogeneity. There are several studies on the use of ADC values to distinguish benign lesions from malignant ones. Lower ADC values have been reported in malignant lesions and infections, compared to normal renal tissues and benign lesions. However, the use of ADC values is restricted, because it is associated with the selected b-values that vary across institutions and protocols.

The analysis of skewness and kurtosis in ADC histograms may describe changes in the tumor microenvironment that are masked in the mean ADC analysis (13-17). In our study, the kurtosis, skewness, and entropy in the ADC histogram analysis were not useful for differentiation of oncocytomas from MRNs. However, there was a significant difference in the mean and median ADC values between the oncocytomas and MRNs. Overall, there are a few reports on the use of ADC values to differentiate the RCC subtypes. Some studies have reported the use of ADC to differentiate the RCC subtypes. It has been shown that ccRCC has a significantly higher ADC compared to other subtypes, whereas a lower ADC has been reported for pRCC. In some reports, ADC was found to be significantly lower in high-grade tumors (III and IV) compared to low-grade clear cell tumors (I and II) in both 1.5 and 3 T MRI systems. However, the routine use of ADC is limited because of institutional differences in diffusion techniques (18, 19).

In the present study, the mean and median ADC values of oncocytomas and ccRCC were similar; therefore, they could not be used for differentiation. The ADC values of oncocytomas, followed by ccRCC, were the highest, whereas the ADC values of pRCC, chRCC, and other renal tumors were the lowest; consequently, we did not differentiate these tumors based on the ADC values. The present study revealed that the ADC values were similar for oncocytomas and ccRCC, which is in line with previous studies reporting difficulties in distinguishing these two tumor subtypes via other imaging methods (20-22).

Cornelis et al. reported that oncocytomas can be differentiated from chRCC and ccRCC using multiparametric MRI (100% and 94.2% specificity, respectively). The multiparametric MRI includes double-echo chemical shift MRI, dynamic contrast-enhanced T1-weighted MRI,

T2-weighted MRI, and ADC maps with the corresponding signal-intensity (SI) index, tumor-to-spleen SI ratio, and ADC ratio in in-phase and out-phase images (23). However, in the current study, we could not differentiate oncocytomas from ccRCC. It should be noted that our findings were based on only DW-MRI, which might have led to the non-differentiation of oncocytomas from ccRCC.

On the other hand, ccRCC could be differentiated from pRCC and chRCC, and oncocytomas could be differentiated from pRCC, chRCC, and other tumors, based on the mean and median ADC values. Besides, the 5th, 10th, 20th, 30th, 40th, 50th, and 60th percentiles of the ADC histogram allowed for the differentiation of ccRCC from pRCC, chRCC, and other tumors ($P < 0.05$), and the 70th, 80th, 90th, and 95th percentiles could differentiate ccRCC from chRCC and other tumors. Conversely, the latter percentiles could not be used to differentiate between ccRCC, oncocytoma, and pRCC.

Kurtosis, skewness, and entropy reflect the tumor heterogeneity. They are first-order parameters, related to the gray-level frequency distribution within the ROI and obtained from the histogram of pixel intensities. Kurtosis depicts the flatness of the histogram and determines the probability distribution; skewness measures asymmetry of the probability distribution; and entropy is a statistical measure of irregularities in a histogram (24-27). These parameters have been used to differentiate ccRCC from pRCC and to assess the RCC stage.

There are studies on the whole-lesion texture analysis to assess low- and high-grade clear cell RCCs. Lower kurtosis and higher skewness on ADC maps have been associated with high-grade ccRCC (17). In the present study, the histogram parameters were not evaluated according to the tumor stage, while the relationship between histogram parameters and different tumor subtypes was examined. Overall, kurtosis, skewness, and entropy were not useful parameters and did not allow differentiation between oncocytoma, ccRCC, pRCC, chRCC, and other tumors.

Young et al. showed that relative corticomedullary signal intensity has high accuracy, sensitivity, and specificity (90%) in differentiation of ccRCC from oncocytomas and other RCC subtypes. Multiphasic MRI enhancement may help differentiate ccRCC from oncocytomas and other RCC types (28). Another study by Hotker et al. showed that a quantitative multiparametric evaluation, involving contrast-enhanced imaging with multiphasic MRI (including peak enhancement, upslope, downslope, and AUC) and chemical-shift indices, was successful in differentiating ccRCC from other renal tumors (29).

In the present study, ccRCC showed higher ADC values than chRCC, pRCC, and other tumors; this finding can help differentiate malignant RCC subtypes. However, clear cell RCC and oncocytomas showed similar ADC values; therefore, the efficacy of ADC analysis in differentiating these tumor subtypes decreased. As reported in a study by Galmiche et al., combined DWI with multiparametric MRI, as dynamic, contrast-enhanced, chemical-shift sequences, may distinguish renal tumor subgroups (30).

There were several limitations to this study. First, it had a retrospective design. Second, histogram analyses were not used to distinguish the tumor grade, because most of the evaluated lesions were grade 2. Third, the number of benign lesions was limited. In the future, standardization of quantitative histogram analysis on ADC maps may be helpful in non-invasive characterization and classification of renal tumor heterogeneity, especially in large study populations.

In conclusion, although differentiation of oncocytomas from ccRCC is not possible by only measuring the mean, median, and peak ADC values and performing a histogram analysis of ADCs, this method can be used effectively to differentiate oncocytomas from MRNs and distinguish MRN subgroups. Overall, the mean, median, and all percentile parameters were superior to kurtosis, skewness, and entropy parameters in the differentiation of MRNs.

Footnotes

Authors' Contribution: Study conception and design: G.E.; acquisition of data: G.E., E.K., B.P., and S.A.; analysis and interpretation of data: G.E., E.K., and B.P.; drafting of the manuscript: G.E. and M.R.G.; critical revision of the manuscript for important intellectual content: M.R.G.; statistical analysis: G.E. and M.R.G.; administrative, technical, and material support: E.K. and S.A.; and study supervision: G.E. and M.R.G.

Conflict of Interests: The authors declare that there is no conflict of interest.

Ethical Approval: KA15/199.

Funding/Support: This study was approved by Baskent University (Ankara, Turkey) Institutional Review Board (Project No.: KA15/199) and funded by Baskent University.

References

1. Ljungberg B, Albiges L, Bensalah K, Bex A, Giles RH, Hora M, et al. *EAU guidelines on renal cell carcinoma 2018*. Arnhem, The Netherlands: European Association of Urology Guidelines Office; 2018.
2. Kim JK, Kim SH, Jang YJ, Ahn H, Kim CS, Park H, et al. Renal angiomyolipoma with minimal fat: differentiation from other neoplasms at double-echo chemical shift FLASH MR imaging. *Radiology*. 2006;**239**(1):174–80. doi: 10.1148/radiol.2391050102. [PubMed: 16507752].

3. Vos N, Oyen R. Renal angiomyolipoma: The good, the bad, and the ugly. *J Belg Soc Radiol*. 2018;**102**(1):41. doi: 10.5334/jbsr.1536. [PubMed: 30039053]. [PubMed Central: PMC6032655].
4. Konety BR, Vaena A, Williams R. Renal parenchymal neoplasms. In: McAninch JW, Lue TF, Smith DR, editors. *Smith and Tanagho's General Urology*. 18th ed. McGraw-Hill Education; 2013.
5. Trinh QD, Saad F, Lattouf JB. The current management of small renal masses. *Curr Opin Support Palliat Care*. 2009;**3**(3):180–5. doi: 10.1097/SPC.0b013e32832e9c6d. [PubMed: 19553818].
6. Maturen KE, Nghiem HV, Caoili EM, Higgins EG, Wolf JJ, Wood DJ. Renal mass core biopsy: Accuracy and impact on clinical management. *AJR Am J Roentgenol*. 2007;**188**(2):563–70. doi: 10.2214/AJR.06.0220. [PubMed: 17242269].
7. Gibbs P, Turnbull LW. Textural analysis of contrast-enhanced MR images of the breast. *Magn Reson Med*. 2003;**50**(1):92–8. doi: 10.1002/mrm.10496. [PubMed: 12815683].
8. Eliat PA, Olivie D, Saikali S, Carsin B, Saint-Jalmes H, de Certaines JD. Can dynamic contrast-enhanced magnetic resonance imaging combined with texture analysis differentiate malignant glioneuronal tumors from other glioblastoma? *Neurol Res Int*. 2012;**2012**:195176. doi: 10.1155/2012/195176. [PubMed: 22203901]. [PubMed Central: PMC3238409].
9. Downey K, Riches SF, Morgan VA, Giles SL, Attygalle AD, Ind TE, et al. Relationship between imaging biomarkers of stage I cervical cancer and poor-prognosis histologic features: Quantitative histogram analysis of diffusion-weighted MR images. *AJR Am J Roentgenol*. 2013;**200**(2):314–20. doi: 10.2214/AJR.12.9545. [PubMed: 23345352].
10. Nowosielski M, Recheis W, Goebel G, Guler O, Tinkhauser G, Kostron H, et al. ADC histograms predict response to anti-angiogenic therapy in patients with recurrent high-grade glioma. *Neuroradiology*. 2011;**53**(4):291–302. doi: 10.1007/s00234-010-0808-0. [PubMed: 21125399]. [PubMed Central: PMC3063200].
11. Wang H, Cheng L, Zhang X, Wang D, Guo A, Gao Y, et al. Renal cell carcinoma: Diffusion-weighted MR imaging for subtype differentiation at 3.0 T. *Radiology*. 2010;**257**(1):135–43. doi: 10.1148/radiol.10092396. [PubMed: 20713607].
12. Somford DM, Hambrock T, Hulsbergen-van de Kaa CA, Futterer JJ, van Oort IM, van Basten JP, et al. Initial experience with identifying high-grade prostate cancer using diffusion-weighted MR imaging (DWI) in patients with a Gleason score </= 3 + 3 = 6 upon schematic TRUS-guided biopsy: a radical prostatectomy correlated series. *Invest Radiol*. 2012;**47**(3):153–8. doi: 10.1097/RLI.0b013e31823ea1f0. [PubMed: 22293513].
13. Chowdhury S, Choueiri TK. Recent advances in the systemic treatment of metastatic papillary renal cancer. *Expert Rev Anticancer Ther*. 2009;**9**(3):373–9. doi: 10.1586/14737140.9.3.373. [PubMed: 19275514].
14. Jamis-Dow CA, Choyke PL, Jennings SB, Linehan WM, Thakore KN, Walther MM. Small (< or = 3-cm) renal masses: Detection with CT versus US and pathologic correlation. *Radiology*. 1996;**198**(3):785–8. doi: 10.1148/radiology.198.3.8628872. [PubMed: 8628872].
15. Hoffmann U, Edwards JM, Carter S, Goldman ML, Harley JD, Zaccardi MJ, et al. Role of duplex scanning for the detection of atherosclerotic renal artery disease. *Kidney Int*. 1991;**39**(6):1232–9. doi: 10.1038/ki.1991.156. [PubMed: 1895675].
16. Kim S, Jain M, Harris AB, Lee VS, Babb JS, Sigmund EE, et al. T1 hyperintense renal lesions: Characterization with diffusion-weighted MR imaging versus contrast-enhanced MR imaging. *Radiology*. 2009;**251**(3):796–807. doi: 10.1148/radiol.2513080724. [PubMed: 19380690].
17. Sandrasegaran K, Sundaram CP, Ramaswamy R, Akisik FM, Rydberg MP, Lin C, et al. Usefulness of diffusion-weighted imaging in the evaluation of renal masses. *AJR Am J Roentgenol*. 2010;**194**(2):438–45. doi: 10.2214/AJR.09.3024. [PubMed: 20093607].
18. Kierans AS, Rusinek H, Lee A, Shaikh MB, Triolo M, Huang WC, et al. Textural differences in apparent diffusion coefficient between low- and high-stage clear cell renal cell carcinoma. *AJR Am J Roentgenol*. 2014;**203**(6):W637–44. doi: 10.2214/AJR.14.12570. [PubMed: 25415729].
19. Taouli B, Thakur RK, Mannelli L, Babb JS, Kim S, Hecht EM, et al. Renal lesions: Characterization with diffusion-weighted imaging versus contrast-enhanced MR imaging. *Radiology*. 2009;**251**(2):398–407. doi: 10.1148/radiol.2512080880. [PubMed: 19276322].
20. Vargas HA, Chaim J, Lefkowitz RA, Lakhman Y, Zheng J, Moskowitz CS, et al. Renal cortical tumors: Use of multiphasic contrast-enhanced MR imaging to differentiate benign and malignant histologic subtypes. *Radiology*. 2012;**264**(3):779–88. doi: 10.1148/radiol.12110746. [PubMed: 22829683]. [PubMed Central: PMC6940015].
21. Hotker AM, Mazaheri Y, Wibmer A, Zheng J, Moskowitz CS, Tickoo SK, et al. Use of DWI in the Differentiation of Renal Cortical Tumors. *AJR Am J Roentgenol*. 2016;**206**(1):100–5. doi: 10.2214/AJR.14.13923. [PubMed: 26700340]. [PubMed Central: PMC4826468].
22. Rosenkrantz AB, Niver BE, Fitzgerald EF, Babb JS, Chandarana H, Melamed J. Utility of the apparent diffusion coefficient for distinguishing clear cell renal cell carcinoma of low and high nuclear grade. *AJR Am J Roentgenol*. 2010;**195**(5):W344–51. doi: 10.2214/AJR.10.4688. [PubMed: 20966299].
23. Cornelis F, Tricaud E, Lasserre AS, Petitpierre F, Bernhard JC, Le Bras Y, et al. Routinely performed multiparametric magnetic resonance imaging helps to differentiate common subtypes of renal tumours. *Eur Radiol*. 2014;**24**(5):1068–80. doi: 10.1007/s00330-014-3107-z. [PubMed: 24557052].
24. Ganeshan B, Abaleke S, Young RC, Chatwin CR, Miles KA. Texture analysis of non-small cell lung cancer on unenhanced computed tomography: Initial evidence for a relationship with tumour glucose metabolism and stage. *Cancer Imaging*. 2010;**10**:137–43. doi: 10.1102/1470-7330.2010.0021. [PubMed: 20605762]. [PubMed Central: PMC2904029].
25. Miles KA, Ganeshan B, Griffiths MR, Young RC, Chatwin CR. Colorectal cancer: Texture analysis of portal phase hepatic CT images as a potential marker of survival. *Radiology*. 2009;**250**(2):444–52. doi: 10.1148/radiol.2502071879. [PubMed: 19164695].
26. Kato H, Kanematsu M, Zhang X, Saio M, Kondo H, Goshima S, et al. Computer-aided diagnosis of hepatic fibrosis: Preliminary evaluation of MRI texture analysis using the finite difference method and an artificial neural network. *AJR Am J Roentgenol*. 2007;**189**(1):117–22. doi: 10.2214/AJR.07.2070. [PubMed: 17579160].
27. Carter JS, Koopmeiners JS, Kuehn-Hajder JE, Metzger GJ, Lakkadi N, Downs LJ, et al. Quantitative multiparametric MRI of ovarian cancer. *J Magn Reson Imaging*. 2013;**38**(6):1501–9. doi: 10.1002/jmri.24119. [PubMed: 23559453]. [PubMed Central: PMC3706562].
28. Young JR, Coy H, Kim HJ, Douek M, Lo P, Pantuck AJ, et al. Performance of relative enhancement on multiphasic MRI for the differentiation of clear cell renal cell carcinoma (RCC) from papillary and chromophobe RCC subtypes and oncocytoma. *AJR Am J Roentgenol*. 2017;**208**(4):812–9. doi: 10.2214/AJR.16.17152. [PubMed: 28125273].
29. Hotker AM, Mazaheri Y, Wibmer A, Karlo CA, Zheng J, Moskowitz CS, et al. Differentiation of clear cell renal cell carcinoma from other renal cortical tumors by use of a quantitative multiparametric MRI approach. *AJR Am J Roentgenol*. 2017;**208**(3):W85–91. doi: 10.2214/AJR.16.16652. [PubMed: 28095036]. [PubMed Central: PMC5441564].
30. Galmiche C, Bernhard JC, Yacoub M, Ravaud A, Grenier N, Cornelis F. Is multiparametric MRI useful for differentiating oncocytomas from chromophobe renal cell carcinomas? *AJR Am J Roentgenol*. 2017;**208**(2):343–50. doi: 10.2214/AJR.16.16832. [PubMed: 27959744].